Journal of Materials Chemistry A

Accepted Manuscript

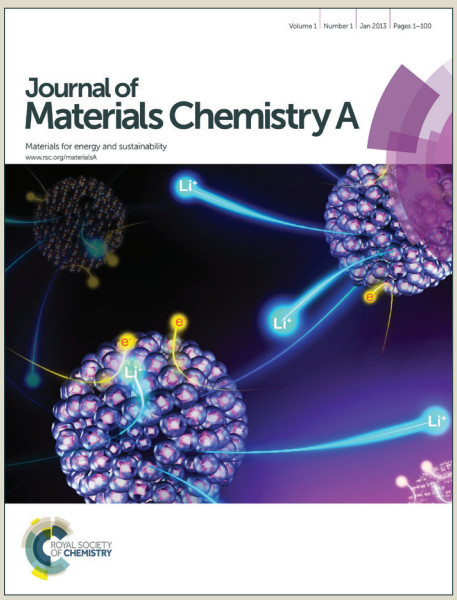

ROYAL SOCIETY OF CHEMISTRY

www.rsc.org/materialsA

Journal of Materials Chemistry A

Cite this: DOI: 10.1039/c0xx00000x

www.rsc.org/xxxxxx

ARTICLE TYPE

A Tin(II) Sulfide/Carbon Anode Material based on Combined Conversion and Alloying Reactions for Sodium-ion Batteries

*Lin Wu,[a] Haiyan Lu,[a] Lifen Xiao, *[b] Jiangfeng Qian,[a] Xinping Ai,[a] Hanxi Yang,[a] and Yuliang Cao *[a]*

Received (in XXX, XXX) Xth XXXXXXXXX 20XX, Accepted Xth XXXXXXXXX 20XX

DOI: 10.1039/b000000x

A tin(II) sulfide/carbon (SnS-C) nanocomposite is prepared by simple high-energy mechanical milling method. XRD, SEM and TEM characterizations show that the nanocomposite is composed of well crystallized SnS nanoparticles with a size of about 15 nm, which are dispersed uniformly in the conductive carbon matrix. The SnS-C electrode exhibits a high Na storage capacity (568 mAh g^{-1} at 20 mA g^{-1}) and excellent cycling stability (97.8% capacity retention over 80 cycles) as well as high-rate capability. *Ex-situ* XRD result testifies a sequential conversion and alloying/dealloing reaction mechanism of the SnS-C electrode during the Na uptaking and extraction cycles. The superior electrochemical performance of the electrodes can be attributed to the small crystalline size of SnS and good carbon coating which facilitate the electrochemical utilization and maintain the structural integrity.

Introduction

The ever-increasing demands of large scale energy storage devices for smart grid as well as vehicle electrification have prompted an extensive search for rechargeable battery systems with high specific energy and low cost. Na ion battery is an attractive battery system with the merits of abundant sodium resources and low environmental impact and has recently intrigued great interest.[1-8] Nevertheless, due to the inherent large size of Na ion (35% much larger than Li ions in radius[1]), the realization of Na ion battery chemistry are hindered by several issues such as sluggish diffusion kinetics of Na ions in the host materials and large volume variation during cycling.

In the past few years, a large variety of cathode materials have been studied for Na ion batteries, including layered metal oxides,[9-11] ferrocyanide,[12] phosphates [13,14] etc. In contrast, the anode materials are mainly limited to hard carbons and metallic alloys. Various hard carbons materials have been surveyed and demonstrated reversible specific capacities less than 300 mAh g^{-1} due to the shorted Na ion accommodations in the carbon structures. Na alloys have higher Li-uptake ability, for example, 300-400 mAh g^{-1} for Na-Sn,[15-19] ca. 600 mAh g^{-1} for Na-Sb,[20-22] ca. 500 mAh g^{-1} Na-SnSb[23] and ca. 1700 mAh g^{-1} Na-P alloys are acquired. [24]

Some metal compounds are Na ion storable through a combined electrochemical conversion and alloying/dealloying mechanism, so as to give superior theoretical capacities (Sb_2O_4: 1227 mAh g^{-1},[25] SnO_2: 1378 mAh g^{-1},[26-29] Sb_2S_3: 946 mAh g^{-1},[30] Sn_3P_4: 1132 mAh g^{-1},[31] SnS: 1022 mAh g^{-1}.[32])when served as anode materials for Na ion batteries. Sun et al. reported that Sb_2O_4 could deliver Na storage capacity of 896 mAh g^{-1} at a low current rate of 1/70 C.[25] But this material can only achieve a capacity of 143 mAh g^{-1} at the current rate of 640 mA g^{-1}, showing very poor rate capability. Su et al. reported a SnO_2@graphene composite, which delivered a reversible capacity of ca. 600 mAh g^{-1} at 20 mA g^{-1}.[29] However, the initial coulombic efficiency of this composite was as low as 32%, probably related to the incomplete recovery of SnO_2 from Sn and Na_2O during charging due to the strong ionic bond of Na-O.[33] Very recently, Yu et al. reported an rGO/Sb_2S_3 composite with a reversible capacity of 730 mAh g^{-1} at 50 mA g^{-1} and an initial coulombic efficiency of 69%.[30] This result indicated that M-S bonds in metal sulfides are weaker than the corresponding M-O bonds in metal oxides, which could be kinetically favorable for the conversion reactions. Thus, we explored the Na storage behavior of tin(II) sulfide (SnS). To the best of our knowledge, although the Li storage behavior of SnS has been investigated previously,[34-36] it is first time that the Na storage performance of SnS is reported in this paper.

Experimental

Samples preparation and characterization

Sn powder (99.8 % purity, -325 mesh, National Medicine CO., Ltd., Shanghai, China), S powders (99.5 % purity, National Medicine CO., Ltd., Shanghai, China) and super P carbon (TIMCAL, Graphite & Carbon Inc.) were used as received. The SnS-C nanocomposite was prepared by high energy mechanical milling (HEMM) under an argon atmosphere for 8 h. The Sn:S was 1:1 by molar ratio, and the SnS:C was 8:2 by weight ratio. For comparison, the Sn-C composite was synthesized by using the same method at a weight ratio of 8:2.

The crystalline structural variation of the electrode upon Na uptaking and extraction was characterized by X-ray diffraction (XRD, Shimadzu XRD-6000). The morphological feature of the SnS-C was investigated using a scanning electron microscopy (SEM, Sirion 2000, FEI) and transmission electron microscopy (TEM, JEOL, JEM-2010-FEF). The samples for TEM analysis were prepared by dispersing the sample powders in ethanol and subsequently releasing a few drops of the dispersed solution on a carbon film supported on a copper grid.

Electrochemical measurements

The SnS-C anodes were prepared by mixing 70 wt% SnS-C composite, 20 wt% super P, and 10 wt% Polyacrylic acid (PAA, 25 wt%) to form a slurry, which was then coated onto a copper (Cu) foil and dried at 60 ^{o}C overnight under vacuum. The charge–discharge performances of the electrode were examined by 2032 coin-type cells using the SnS-C anode as a working electrode and a Na disk as counter electrode, 1 M $NaPF_6$ dissolved in ethylene carbonate (EC)/diethyl carbonate (DEC) (1:1 by volume) as the electrolyte, and the separator was a microporous membrane (Celgard 2400). The Na disks were home-made by rolling sodium lumps into thin plate, and then cut into circulated disks. All the cells were assembled in a glove box with water/oxygen content lower than 1 ppm and tested at room temperature. The loading of the active material in the electrode is about 2.0 mg cm^{-2}. The galvanostatic charge–discharge test was conducted on a LAND cycler (Wuhan Kingnuo Electronic Co., China). The discharge/charge capacity was calculated based on the SnS mass in the composites. Cyclic voltammetric measurements were carried out with the coin cells at a scan rate of 0.1 mV s^{-1} using a CHI 660 c electrochemical workstation (ChenHua Instruments Co., China).

Results and Discussion

Structural and morphological characterizations

Figure 1 presents the morphologic and structural characterization of the SnS-C nanocomposite after HEMM. It can be observed from the SEM image that the as prepared material appears as uneven agglomerates (Fig. 1a). TEM image shows that agglomerates consist of a lot of primary crystalline nanoparticles (Fig. 1b). High-resolution TEM (HRTEM) image (Fig. 1c) revealed that the nanocrystallines have fine lattice fringes with distances of 0.342 nm and 0.282 nm, corresponding well to the (120) and (111) plane of the orthorhombic SnS (JPCDS no. 39-0354), respectively. The SnS nanoparticles are about 15 nm in size and are embedded uniformly in the amorphous carbon matrix. This unique structure can not only provide good electric conductivity, but also buffer effectively the volumetric variation during the Na uptaking and extraction processes. Fig. 1d gives the experimental XRD patterns of the SnS-C and Sn-C nanocomposites. It shows that all the diffraction peaks of the SnS-C nanocomposite can be well indexed to the orthorhombic SnS phase (JPCDS no. 39-0354). No impurities of primary Sn or S can be detected. Therefore, the TEM and XRD characterizations prove the complete transformation of Sn and S into SnS after HEMM. For comparison, all the diffraction peaks of the Sn-C nanocomposite can be indexed to the tetragonal Sn phase (JPCDS no. 04-0673). The average crystalline sizes of SnS and Sn are 15 and 30 nm in the SnS-C and Sn-C nanocomposites, calculated from the FWHM of the (120) peak (SnS) and (101) peak (Sn) respectively. The smaller crystalline size of SnS should benefit the electrochemical utilization and structural integration more than that of Sn.

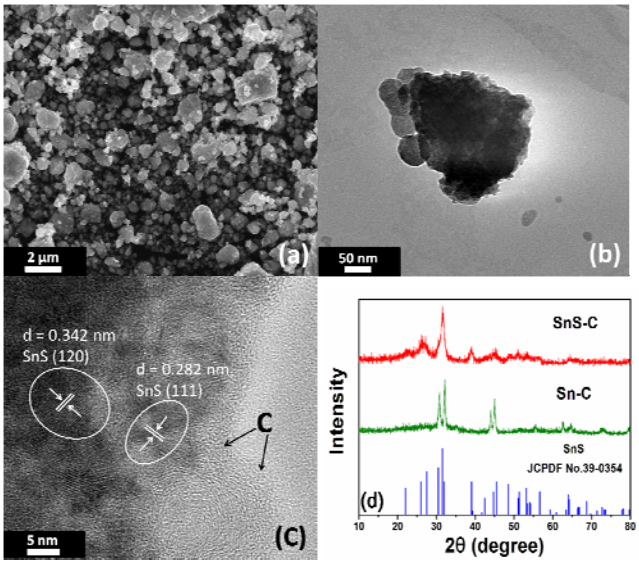

Figure 1. (a) SEM image of the SnS-C nanocomposite; (b) TEM image of the SnS-C nanocomposite; (c) High resolution TEM image of the SnS-C nanocomposite; (d) XRD patterns of the SnS-C and Sn-C nanocomposites.

Electrochemical performances of Sn-C nanocomposite

Figure 2a shows the typical CV curves of the SnS-C electrode (the scan rate is set at 0.1 mV s^{-1}). The first negative scan shows three reductive peaks positioned at 0.62, 0.5 V and 0.0 V. The peaks occurring at 0.62 and 0.5 V is observed to shift positively to 0.98 and 0.66 V respectively at the second negative scan, implying that an activation process occurs at the first scan.[20] Besides, the reductive current peak area of the first scan is much larger than that of the second scan, indicating an irreversible decomposition of the electrolyte to form solid electrolyte interface (SEI) layer during the initial sodiation process. On the reverse positive scan, three oxidative peaks can be observed at 0.31, 0.71 and 1.09 V. According to the previous reports,[16,23] Na-Sn alloying-dealloying reaction occurs at a relatively low potential range of below 0.8 V, so the two pairs of redox peaks positioned at 0.31/0 V and 0.71/ 0.66 V at the second scan should correspond to the alloying/dealloying reactions of Sn with Na. The third pair of redox peaks centered at 1.09/0.98 V therefore should be attributed to the conversion reaction of SnS to Sn and Na_2S, analogous to the conversion reaction of SnS to Sn and Li_2S as used as Li-uptake anode. As a result, when SnS is used as anode for Na ion batteries, the electrochemical reactions should include two successive steps as following:

$$SnS + 2Na^+ + 2e^- \Leftrightarrow Na_2S + Sn \quad (1)$$

$$Sn + 3.75Na^+ + 3.75e^- \Leftrightarrow Na_{3.75}Sn \quad (2)$$

According to the above reactions, the overall theoretical capacity of SnS used as anode for Na ion batteries is 1022 mAh g^{-1} (355 mAh g^{-1} is ascribed to the conversion reaction described by eqn (1) and 667 mAh g^{-1} to the alloying-dealloying reaction described by eqn (2)).

Figure 2b compares the initial discharging-charging curves of the SnS-C and Sn-C electrodes at a constant current density of 20 mA g^{-1}. In the case of the Sn-C electrode, most of the discharge capacity occurs below 0.5 V, indicating that the Na-Sn alloying reaction occurs at a relatively low potential range, agreeing well with the previous report.[37] The initial reversible capacity of the

Sn-C electrode is 394 mAh g^{-1}, corresponding to 46.5 % of the theoretical capacity of $Na_{3.75}Sn$ (846 mAh g^{-1}), indicating a sluggish kinetic of Sn in the alloying reaction. In contrast, a pair of short potential plateaus can be clearly visualized between 0.8 and 1.1 V at the discharging-charging curves of the SnS-C electrode, which should be ascribed to the conversion reaction described by eqn (1). The SnS-C electrode recovers a reversible capacity of 325 mAh g^{-1} above 0.8 V, equivalent to 92 % of the theoretical capacity of eqn (1), indicating the conversion reaction between SnS and Na_2S+Sn is highly reversible. The SnS-C electrode offers a reversible capacity of 568 mAh g^{-1} during the whole charging potential range, which is much less than the theoretical capacity (1022 mAh g^{-1}) based on eqn (1) and eqn (2). Thus, only a small part of the freshly generated Sn nanograins from the conversion reaction participates in the subsequent alloying reaction. The initial coulombic efficiency of the SnS-C electrode is 66 %, much higher than that (32 %) of SnO_2 electrode,[29] which should benefit from the higher conversion efficiency of Na_2S to SnS than Na_2O to SnO_2.

Figure 2c compares the rate capability of the Sn-C and SnS-C electrodes. The SnS-C electrode offered a reversible capacity of 568, 546, 544, 524 493 and 452 mAh g^{-1} at the charging-discharging current density of 20, 50, 100, 200, 400 and 800 mA g^{-1}, respectively. As can be seen, even at a very high rate of 800 mA g^{-1}, the SnS-C electrode can still deliver 80 % of the capacity obtained at 20 mA g^{-1}. In contrast, the Sn-C electrode can only recover a capacity of 120 mAh g^{-1} at 800 mA g^{-1}, corresponding to 28% of that obtained at 20 mA g^{-1}. The excellent rate capability of the SnS-C electrode may originate from the smaller SnS nanoparticles and the tightly connected carbon matrix formed during HEMM, which is beneficial to the improvement of the reaction kinetic and electronic conductivity.

Figure 2d compares the cycling performances of the Sn-C and SnS-C electrode at a current density of 100 mA g^{-1}. The SnS-C electrode exhibits a much higher sodium uptaking capacity than that of the Sn-C electrode, owing to the extra capacity from the conversion reaction. Both electrodes show a capacity increase during the initial several cycles. This indicates that both electrodes have undergone an activation process, such as gradually improved wetting of the electrode by the electrolyte or the structural rearrangement of the active material, leading to enhanced electrochemical utilization. The capacity of the Sn-C electrode increases first, and then decreases slowly during prolonged cycles. In contrast, the reversible capacity of the SnS-C first increases from 486 to 548 mAh g^{-1}, then maintains almost stable. The SnS-C electrode demonstrates a capacity retention of 97 % over 80 cycles, much higher than that (59 %) of the Sn-C electrode. The better cyclability of the SnS-C electrode should benefit from the strong buffering effect of the Na_2S matrix generated through the conversion reaction, which surrounds closely the Sn nanoparticles to prevent it from aggregating during repeated charging and discharging.[16] Though the coulombic efficiency of the SnS-C electrode is 65 % in the first cycle, it increases rapidly to > 99 % at the 5th cycle and then remains steady over the subsequent cycles, indicating excellent reversibility of the conversion as well as the alloying-dealloying processes.

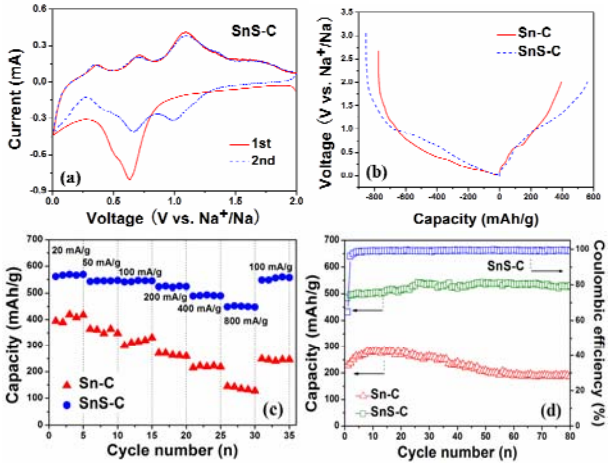

Figure. 2 (a) Initial two cyclic voltammogram curve (CV) of the SnS-C nanocomposite electrode from 2.00 V to 0.01 V vs. Na^+/Na at a scan rate of 0.1 mV s^{-1}; (b) The initial discharge/charge profiles of the SnS-C and Sn-C electrodes between 0.01 V and 2.0 V vs. Na^+/Na at a current rate of 20 mA g^{-1}; (c) Rate capability of the SnS-C and Sn-C electrodes at various current rates from 20 to 800 mA g^{-1}; (d) Cycling performance of the SnS-C and Sn-C electrodes at a cycling rate of 100 mA g^{-1}.

In order to further confirm the conversion and alloying-dealloying mechanism described above, *ex-situ* XRD was conducted to characterize the phase variation of the electrodes at different charging and discharging states during the first cycle (as shown in Figure 3). The fresh electrode presents a typical diffraction pattern of the crystalline SnS (Figure 3a). After discharged to 0.6 V (Figure 3b), the characteristic peaks associated to SnS disappears completely. A new set of diffraction peaks located at 30°, 32° and 45° appears, which can be denoted to the crystalline Sn (JCPDS no. 04-0673). After fully discharged to 0.01 V (Figure 3c), a peak positioned at 35° can be well assigned to Na_2S phase (JCPDS no. 47-0178), and two peaks centered at 33.3° and 53° are corresponding to the $Na_{15}Sn_4$ new phase (JCPDS no. 31-1327). Thus, the *ex-situ* XRD clearly demonstrates SnS goes through a conversion and alloying cascade reaction during Na uptaking process. Besides, it is noted that after discharged to 0.01 V, the diffraction peaks arising from Sn phase have not disappeared but the intensity attenuates when discharged to 0.01 V. This result again verifies that the newly formed Sn phase from the conversion reaction can not entirely react with Na during the first Na uptaking process, as shown in Figure 2b. When the electrode is recharged to 0.8 V (Figure 3d), the crystalline $Na_{15}Sn_4$ alloy phase disappears indicating that the dealloying reaction has completed. After the electrode is recharged to 2.0 V, no diffraction peaks apart from those arising from Cu collector are observed, indicating that Sn is converted to amorphous or very small SnS nanoparticles which cannot be captured by XRD measurement. Thus, the ex-situ XRD pattern evidently demonstrates that sequential conversion and alloying reactions occurring during Na uptaking and extraction cycles.

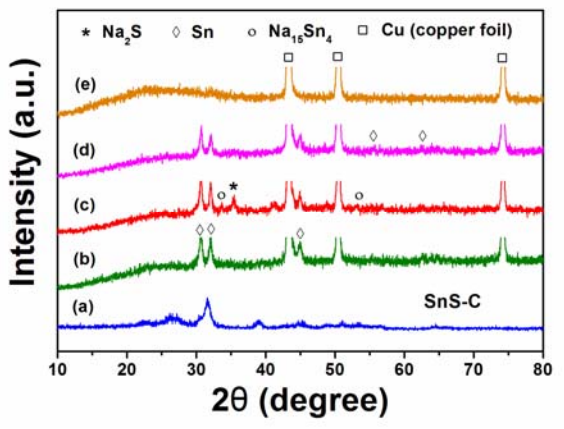

Figure. 3 *Ex-situ* XRD patterns of the SnS-C electrode at different discharging and charging states, (a) fresh electrode; (b) after 1st discharging to 0.6 V; (c) after 1st discharging to 0.01 V; (d) after 1st charging to 0.8 V; (e) after 1st charging to 2.0 V.

Conclusions

In summary, SnS-C nanocomposite was synthesized by a simple high-energy mechanical milling method. XRD, SEM and TEM characterizations demonstrated that well crystallized and highly pure SnS nanoparticles were produced and uniformly dispersed in the conductive carbon matrix. The CV and charging-discharging tests showed that SnS underwent a complete conversion reaction to form Na_2S and Sn phase, then a part of newly formed Sn was alloyed with Na during the Na uptaking process and vice verse during Na extraction process. This electrochemical reaction sequence was also verified by *Ex-situ* XRD investigation. The as prepared SnS-C electrode delivered a higher reversible capacity (568 mAh g^{-1} at 20 mA g^{-1}) and better cycling stability as well as higher rate capability compared to that of the Sn-C electrode. The superior electrochemical performances could be ascribed to the small crystalline size of the SnS active material, the buffering effect of in-situ formed Na_2S nanograins and the good conductive carbon coating.

Acknowledgements

We thank financial support by the National Science Foundation of China (No. 21173160, No. 2133307 and No. 21373155) and Program for New Century Excellent Talents in University (NCET-12-0419).

Notes and references

a Hubei Key Lab. of Electrochemical Power Sources, College of Chemistry and Molecular Science, Wuhan University, China. E-mail: ylcao@whu.edu.cn;

b College of Chemistry, Central China Normal University, Wuhan 430079, China. E-mail: lfxiao@mail.ccnu.edu.cn.

1 M.D. Slater, D. Kim, E. Lee, C.S. Johnson, *Adv. Funct. Mater.* , 2013, **23**, 947.
2 S.W. Kim, D.H. Seo, X. Ma, G. Ceder, K. Kang, *Adv. Energy Mater.* , 2012, **2**, 710.
3 V. Palomares, P. Serras, I. Villaluenga, K.B. Hueso, J. Carretero-Gonzalez, T. Rojo, *Energy Environ. Sci.*, 2012, **5**, 5884.
4 A. Ponrouch, E. Marchante, M. Courty, J.M. Tarascon, M.R. Palacin , *Energy Environ. Sci.*, 2012, **5**, 8572.
5 S. Komaba, T. Ishikawa, N. Yabuuchi, W. Murata, A. Ito, Y. Ohsawa, *ACS Appl. Mat. Interfaces*, 2011, **3**, 4165.
6 S.Y. Hong, Y. Kim, Y. Park, A. Choi, N.S. Choi, K.T. Lee, *Energy Environ. Sci.*, 2013, **6**, 2067.
7 S.P. Ong, V.L. Chevrier, G. Hautier, A. Jain, C. Moore, S. Kim, X. Ma, G. Ceder, *Energy Environ. Sci.*, 2011, **4**, 3680.
8 H. Pan, Y.S. Hu, L. Chen, *Energy Environ. Sci.*, 2013, **6**, 2338.
9 Y. Cao, L. Xiao, W. Wang, D. Choi, Z. Nie, J. Yu, L.V. Saraf, Z. Yang, J. Liu, *Adv. Mater.*, 2011, **23**, 3155.
10 D. Kim, S.H. Kang, M. Slater, S. Rood, J.T. Vaughey, N. Karan, M. Balasubramanian, C.S. Johnson, *Adv. Energy Mater.*, 2011, **1**, 333.
11 D. Yuan, X. Liang, L. Wu, Y. Cao, X. Ai, J. Feng, H. Yang, *Adv. Mater.* **2014**, DOI: 10.1002/adma.201401946.
12 J. Qian, M. Zhou, Y. Cao, X. Ai, H. Yang, *Adv. Energy Mater.*, 2012, **2**, 410.
13 H. Kim, I. Park, D.H. Seo, S. Lee, S.W. Kim, W.J. Kwon, Y.U. Park, C.S. Kim, S. Jeon, K. Kang, *J. Am. Chem. Soc.*, 2012, **134**, 10369.
14 Y. Fang, L. Xiao, J. Qian, X. Ai, H. Yang, Y. Cao, *Nano Lett.* **2014,** *14* (6), 3539-3543.
15 H. Zhu, Z. Jia, Y. Chen, N. Weadock, J. Wan, O. Vaaland, X. Han, T. Li, L. Hu, *Nano Lett.*, 2013, **13**, 3093.
16 L. Wu, X. Hu, J. Qian, Pei, F. F. Wu, R. Mao, X. Ai, H. Yang, Y. Cao, *J. Mater. Chem. A*, 2013, **1**, 7181.
17 Y. Xu, Y. Zhu, Y. Liu, C. Wang, *Adv. Energy Mater.*, 2012, **3**, 128-133.
18 M.K. Datta, R. Epur, P. Saha, K. Kadakia, S.K. Park, P.N. Kumta, *J. Power Sources*, 2013, 225, 316.
19 S. Komaba, Y. Matsuura, T. Ishikawa, N. Yabuuchi, W. Murata, S. Kuze, *Electrochem. Commun.*, 2012, **21**, 65.
20 L. Wu, X. Hu, J. Qian, F. Pei, F. Wu, R. Mao, X. Ai, H. Yang, Y. Cao, *Energy Environ. Sci.*, 2014, **7**, 323.
21 J. Qian, Y. Chen, L. Wu, Y. Cao, X. Ai, H. Yang, *Chem. Commun.*, 2012, **48**, 7070.
22 L. Wu, F. Pei, R. Mao, F. Wu, Y. Wu, J. Qian, Y. Cao, X. Ai, H. Yang, *Electrochim. Acta*, 2013, **87**, 41.
23 L. Xiao, Y. Cao, J. Xiao, W. Wang, L. Kovarik, Z. Nie, J. Liu, *Chem. Commun.*, 2012, **48**, 3321.
24 J. Qian, X. Wu, Y. Cao, X. Ai, H. Yang, *Angew. Chem. Int. Ed.*, 2013, **52**, 4633.
25 Q. Sun, Q.Q. Ren, H. Li, Z.W. Fu, *Electrochem. Commun.*, 2011, **13**, 1462.
26 M. Gu, A. Kushima, Y. Shao, J.G. Zhang, J. Liu, N.D. Browning, J. Li, C. Wang, *Nano Lett.*, 2013, **13**, 5203.
27 Y.X. Wang, Y.G. Lim, M.S. Park, S.L. Chou, J.H. Kim, H.K. Liu, S.X. Dou, Y.J. Kim, *J. Mater. Chem. A*, 2014, 2, 529.
28 Y. Wang, D. Su, C. Wang, G. Wang, *Electrochem. Commun.*, 2013, **29**, 8.
29 D. Su, H.J. Ahn, G. Wang, *Chem. Commun.*, 2013, **49**, 3131.
30 D.Y.W. Yu, P.V. Prikhodchenko, C.W. Mason, S.K. Batabyal, J. Gun, S. Sladkevich, A. G. Medvedev, O. Lev, *Nat. Commun.*, 2013, **4**.
31 J. Qian, Y. Xiong, Y. Cao, X. Ai, H. Yang, *Nano Lett.*, 2014, **14**, 1865.
32 B. Qu, C. Ma, G. Ji, C. Xu, J. Xu, Y.S. Meng, T. Wang, J.Y. Lee, *Adv. Mater.*, 2014.
33 D.L. Hildenbrand, *E. Murad, J. Chem. Phys.*, 1970, 53, 3403.
34 J.G. Kang, J.G. Park, D.W. Kim, *Electrochem. Commun.*, 2010, **12**, 307.
35 J. Lu, C.Nan, L. Li, Q. Peng, Y. Li, *Nano Res.*, 2013, **6**, 55.
36 D.D. Vaughn, O.D. Hentz, S. Chen, D. Wang, R.E. Schaak, *Chem. Commun.*, 2012, **48**, 5608.
37 L.D. Ellis, T.D. Hatchard, M.N. Obrovac, *J. Electrochem. Soc.*, 2012, **159**, A1801.

A table of contents entry

Title: A Tin(II) Sulfide/Carbon Anode Material based on Combined Conversion and Alloying Reactions for Sodium-ion Batteries

Lin Wu, Haiyan Lu, Lifen Xiao, Xinping Ai, Hanxi Yang and Yuliang Cao

TOC figure:

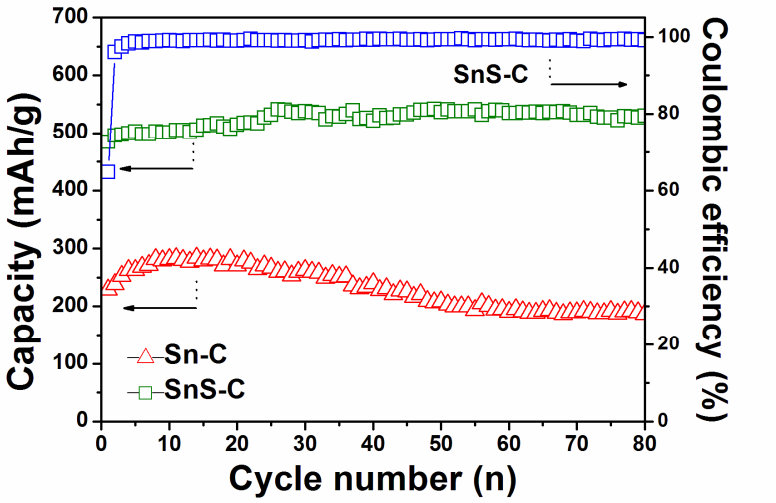

SnS-C nanocomposite can deliver a high capacity (568 mAh g^{-1}) for Na storage based on the conversion and alloying reaction.